Dynamic range and sensitivity improvement in near-infrared detectors using silicon germanium bipolar complementary metal-oxide semiconductor technology

Johan Venter
Saurabh Sinha
University of Pretoria
Carl and Emily Fuchs Institute for Microelectronics
Department of Electrical, Electronic and Computer
    Engineering
Pretoria, South Africa
E-mail: jwventer@ieee.org

Abstract. Classically gated infrared (IR) detectors have been implemented using charge-coupled devices (CCD). Bipolar complementary metal-oxide semiconductor (BiCMOS) technology emerged as a viable alternative platform for development. BiCMOS technology has a number of advantages over CCD and conventional CMOS technology, of which increased switching speed is one. The pixel topology used in this work is a reversed-biased diode connected heterojunction bipolar transistor. The disadvantage of CMOS detectors is the increased readout noise due to the increased on-chip switching compared to CCD, which degrades dynamic range (DR) and sensitivity. This yields increased switching speeds compared to conventional bipolar junction transistors. Sensitivity improved from 50 mA/W (peak) at 430 nm in CCD detectors to 180 mA/W (peak) (or 180,000 V/W) at 665 nm in BiCMOS detectors. Other CMOS IR detectors previously published in the literature showed sensitivity values from 2750 to 5000 V/W or 100 mA/W. The DR also improved from 47 and 53 dB to 70 dB. The sensitivity of conventional CCD detectors previously published is around 53 mA/W. The second advantage is that detection in the near-IR band with conventional silicon integrated technology is possible. This work has shown increased detection capabilities up to 1.1 μm compared to Si detectors. © 2013 Society of Photo-Optical Instrumentation Engineers (SPIE) [DOI: 10.1117/1.OE.52.4.044001]

Subject terms: charge-coupled devices; heterojunctions; infrared; detectors; noise; photodetectors.

Paper 121891 received Dec. 30, 2012; revised manuscript received Mar. 5, 2013; accepted for publication Mar. 11, 2013; published online Apr. 3, 2013.

1 Introduction

Gated infrared (IR) imaging is used in a variety of specialized applications and has shown significant progress.[1–6] These detectors are commonly implemented with charge-coupled devices (CCD). The CCD sensors are bulky and consume more power compared to their bipolar complementary metal-oxide semiconductor (BiCMOS) equivalent. CCD detectors exhibit high dynamic range (DR) and sensitivity. The disadvantage is that they only detect radiation in a small part of the near-IR range. BiCMOS detectors have shown improvements over CCD detectors because they have lower power consumption, high speed operation, and lower manufacturing cost.[2–4] Several IR detectors have been reported in the literature, but are not amenable to integration in a single Si chip because nonsilicon materials such as gallium arsenide and indium gallium arsenide are commonly used in those applications.[7]

Silicon (Si), a commonly available and cheap platform for detector development, exhibits band gap energy of 1.17 eV, which makes this an unsuitable material for near-IR development. Other materials exist that can detect IR radiation effectively, but they are difficult to integrate with other systems because of large donor atom sizes compared to Si, as well as commonly available manufacturing processes. Methods such as the microelectromechanical system (MEMS) processes, together with materials such as indium gallium arsenide, are commonly used to achieve IR detection with Si integrated technology with a trade-off of repeatability in mass production, which in turn increases cost.[7] Germanium (Ge) exhibits band gap energy of 0.66 eV, which can detect near- to mid-IR radiation with ease.[8] This is a cheaper way of prototyping BiCMOS IR detectors owing to increased repeatability which decreases cost of production.

A major problem in detector design using BiCMOS technology is the inherent noise[6,9] that the detector exhibits in comparison to CCD detectors, which is shown in Eqs. (1) and (2). This on-chip noise degrades the performance of these detectors. The peripheral circuitry in CCD detectors is usually implemented off-chip, whereas in the case of (Bi)CMOS detectors it is usually implemented on-chip.

2 Impact of Noise in Gated (Bi)CMOS Detectors

This section outlines the role that noise plays in detectors. The following section describes the contributors to noise and then a discussion on noise contribution in DR and sensitivity follows.

2.1 Noise Contributors

There are several contributors to noise in BiCMOS IR detectors. These range from Johnson noise to fixed pattern noise. Noise decreases the DR and sensitivity in a system. Several different techniques exist to eliminate some of these noise contributors. These can be divided into two categories.

Table 1 Published noise values in detectors.

Reference	11	12	13
Technology node	0.35 μm CMOS	0.18 μm CMOS	0.13 μm CMOS
Noise	0.76 μV/$\sqrt{\text{Hz}}$	72 μV/$\sqrt{\text{Hz}}$	50 nV/$\sqrt{\text{Hz}}$

The first one is readout circuit techniques, such as the source follower and the shared pixel readout circuit.[4,10] The second category is the type of pixel element used. The best type of element to use is the p-i-n diode. Table 1 describes some published noise values in the literature.

The large variance in the values is due to the different topologies used.

2.2 Dynamic Range

DR is the ratio of the pixel saturation level to its signal threshold. The threshold is usually dominated by noise currents. These can be calculated by two equations. When integration time, dark current, and photon-generated current are not taken into account, DR can be calculated by Eq. (1):[14]

$$\text{DR} = \frac{V_{\text{MAX}} - V_{\text{DARK}}}{\sqrt{V^2_{\text{NOISE}_{\text{DARK}}} + 2\frac{kT}{\alpha q}G_{C_{\text{PH}}} + \frac{V^2_{\text{READOUT}_{\text{NOISE}}}}{A^2_{\text{TOT}}}}}, \quad (1)$$

where V_{MAX} is the maximum output voltage of the IR detector, V_{DARK} is the dark voltage output, $V^2_{\text{NOISEDARK}}$ is the dark noise voltage, k is Boltzmann's constant (8.617×10^{-5} eV/K), T is the temperature (K), α is a coefficient between 1 and 2. $\alpha \approx 1$ in hard reset mode and $\alpha \approx 2$ in soft reset, q is the charge of an electron (1.602×10^{-19} C), G_{CPH} is the conversion gain, $V^2_{\text{READOUTNOISE}}$ is the readout noise of the detector, and A_{TOT} is the readout circuit gain. There is no wavelength-dependent parameter in Eq. (1), therefore it is conducive for practical measurements. Figures 1 and 2 show the setup to obtain experimental values for this parameter.

When integration time, dark current, and photon-generated current are taken into account, DR can be calculated by Eq. (2):[15]

$$\text{DR}_{\text{dB}} = 20 \log \frac{qQ_{\text{well}} - i_{\text{DC}}\tau_{\text{INT}}}{\sqrt{qi_{\text{DC}}\tau_{\text{INT}} + q^2(\sigma^2_{\text{read}} + \sigma^2_{\text{DSNU}})}}, \quad (2)$$

where i_{PH} is the photon-generated current (A), i_{DC} is the dark current present (A), τ_{INT} is the integration time (s), σ^2_{read} is the
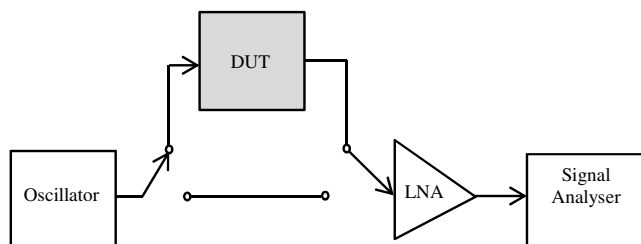

Fig. 1 Block diagram of the experimental setup for noise measurements.
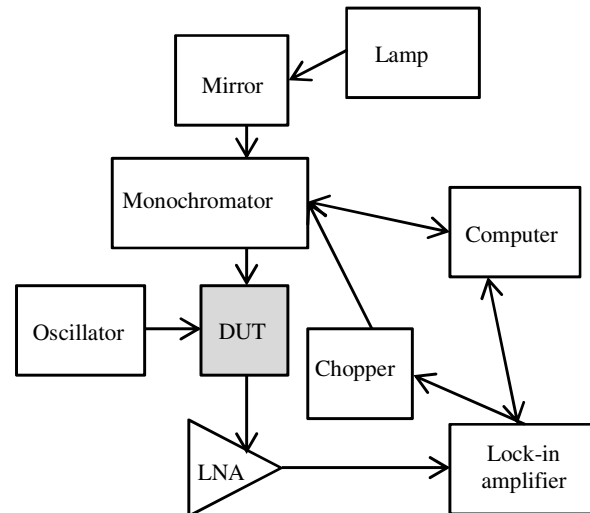

Fig. 2 Block diagram of the experimental setup for the sensitivity measurements.

detector noise, σ^2_{DSNU} is the dark signal nonuniformity, and Q_{well} is the well capacity just before the detector saturates.

As seen in both Eqs. (1) and (2), noise is the primary degrading factor. Many efforts have been made to reduce the different noise contributors and in some cases eliminate certain contributors. Table 2 describes some published DR values.

Table 2 shows that the average DR achieved is around 50 dB. This is due to the higher noise that p-i-n diodes exhibit.

2.3 Sensitivity

The sensitivity (Sens) of an IR detector can be calculated practically using Eq. (3):[11]

$$\text{Sens} = \frac{S}{P \times A}, \quad (3)$$

where S is the signal output (in V or A), P is the intensity of the radiated wave (W/cm^2) and A is the sensitive area of the detector (cm^2). The disadvantage with Eq. (3) is that only the sensitivity of one specific setup can be simulated. No frequency-dependent parameter is included. The photon-induced current of an IR detector under illumination is given in Eq. (4):[15,18]

$$i_{\text{PH}} = \frac{q\lambda}{\text{hc}}P_{\text{i}}(1 - e^{-\alpha_S w})(1 - R_f), \quad (4)$$

where q is the electron charge (1.602×10^{-19} C), h is Planck's constant (4.135×10^{-15} eV.s), c is the speed of

Table 2 Published DR values.

Reference	16	17
Technology node	0.18 μm CMOS	0.13 μm CMOS
DR	54 dB	47 dB

Table 3 Published sensitivity values.

Reference	11	12	16	17	13
Technology node	0.35 μm CMOS	0.18 μm CMOS	0.18 μm CMOS	0.13 μm CMOS	0.13 μm CMOS
Sensitivity	4970 V/W	0.1 A/W	2750 V/W	26.8 mV/dB	5000 V/W

light 3×10^8 m/s, λ is the radiating wavelength (m), P_i is the incident energy (W), α_s is the absorption coefficient, w is the width of the undoped region (in the case of Si p-i-n diodes) or the width of the base of the heterojunction bipolar transistor (HBT) (in the case of the SiGe HBT) (m), and R_f is the reflection coefficient. The sensitivity of an IR detector can be calculated by rearranging Eq. (4) such that i_{PH}/P_i is on left side which is then equal to the sensitivity of the detector in terms of absorption coefficients, width of the base of the heterojunction and reflection coefficient.

Noise also degrades the sensitivity of an IR detector. The S term in Eq. (3) is the amount of output swing (in volt or ampere) from its stationary point, which is the noise. Table 3 describes some sensitivity values published in the literature.

Table 3 shows that the average sensitivity achieved in the literature is around 5000 V/W. Sufficient information is not available in any of the publications mentioned to enable comparison of the detectors using the A/W rating. Nonetheless, this gives a fair indication of what has been achieved.

3 Commonly Used Photodetector Material

Table 4 shows the most commonly used photodetector materials.

Table 4 shows that there are several materials that can detect radiation in the IR band. The disadvantage is that the materials that do not include Si are not easily capable of being integrated with Si integrated technology, on which most integrated solutions are based. Since Si can only detect radiation in the visible band and cuts off just before the near-IR band, it has proven to be a challenge to realize gated IR detectors monolithically.

Table 4 Summary of the most commonly used materials in photodetectors.[8]

Type	E_G (eV)	λ_c (nm)	Band
Silicon	1.12	1100	Visible
Gallium arsenide	1.42	875	Visible
Germanium	0.66	1800	Near-infrared
Indium gallium arsenide	0.73 to 0.47	1700 to 2600	Near-infrared
Indium arsenide	0.36	3400	Near-infrared
Indium antimonide	0.17	5700	Mid-infrared
Mercury cadmium telluride	0.7 to 0.1	1700 to 12500	Near- to far-infrared

4 Effect of Base Doping in HBT

Si exhibits band gap energy of 1.17 eV corresponding to a cut-off wavelength of 1.1 μm, whereas Ge exhibits band gap energy of 0.66 eV with a corresponding cut-off wavelength of 1.8 μm. A hybrid of the two materials will have a cut-off wavelength between the two extremes. Figure 3 shows the effect of different levels of Ge doping in Si wafers.

Figure 3 shows the quantum efficiency (QE) of $Si_{1-x}Ge_x$ detectors. These values were plotted from experimentally obtained absorption coefficients from Virginia Semiconductor.[19] As seen in Fig. 3, the doping fraction of 0 and 0.25 intersects. Upon further inspection by using theoretical absorption coefficients, this intersection was attributed to a possible instrumental error. No post-processing was performed in this simulation. A shift to the near-IR band occurs as the doping levels of Ge increase. This shift is due to the β-multiplication effect the Ge doping introduces in HBTs owing to decreased base resistance. Several high-quality near- to mid-IR detectors that make use of Si have been described in the literature. Most of these Si detectors are quantum dots, which are not easily integrated with Si electronics. Thus, the challenge is to develop detectors that are integrated with conventional Si-based technologies; one solution is presented in this paper. One feasible material commonly used for uncooled detectors is silicon germanium (SiGe).[7]

5 Pixel Design

Ge exhibits lower band gap energy compared to Si, as shown in Table 4. Therefore, the structure of the detector should be designed in such a way that the electrons move from a high energy band gap to a lower energy band gap. With regards to this work, the technology node from ams AG (formerly
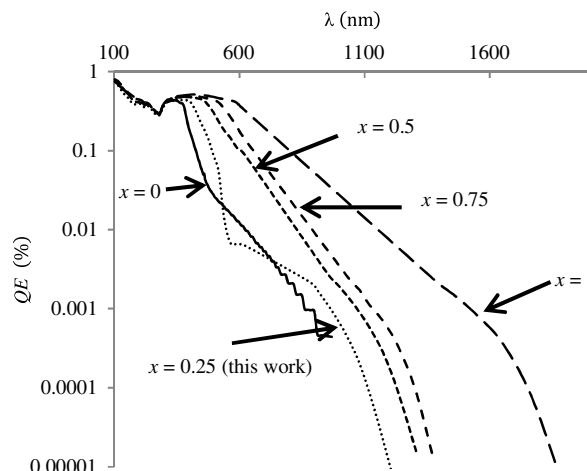

Fig. 3 Quantum efficiency (QE) of Si with different levels of Ge doping.

known as Austriamicrosystems) has limitations as to what can be prototyped on chip. Commonly used techniques in MEMS processes, such as barrier profiling, are not typically employed for a multi-project wafer (MPW), the approach used for prototyping this work. The most common way of prototyping detectors is with the p-i-n diode. Only Si can be used with the p-i-n diode, which has the inherent problem of high band gap that makes near-IR detection difficult.

The only other structure that makes no design rule check errors in this process is the diode-connected HBT structure, which has some Ge doped in the base of the transistor. Figure 4 shows the cross-section of an HBT.

As mentioned above, the base is doped with Ge, which is shown in Fig. 4. Figure 5 shows how the pixels were formed by simply connecting the base and the emitter with a metal wire.

In Fig. 5 it can be seen that the pixel diode is formed between the collector and base to increase the detection area. This doping not only increases the inherent gain in the pixel, it also shifts the detecting band to the near-IR band. The theory that verifies this can be explained by analyzing the band gap energy diagram of the diode-connected HBT structure, which is given in Fig. 6.

Figure 6 shows the band gap energy diagram of the reversed-biased diode-connected SiGe HBT detector. The addition of Ge reduces the band gap, which then shifts the detecting band to the near-IR band. As seen in Fig. 3, increasing the Ge doping within the allowable limits aids in reducing the band gap. This shifts the detecting band even further into the IR band.
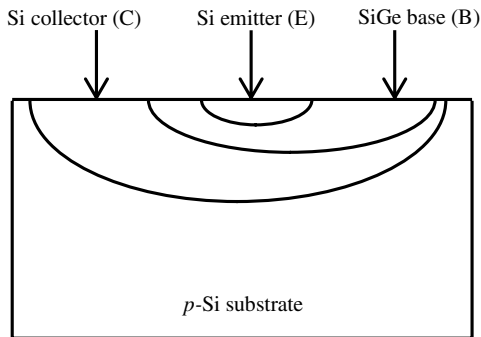

Fig. 4 Cross-section of an on-chip implementation of an heterojunction bipolar transistor (HBT).
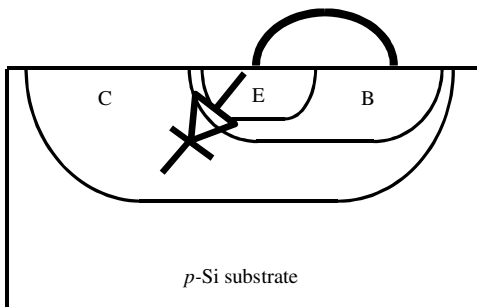

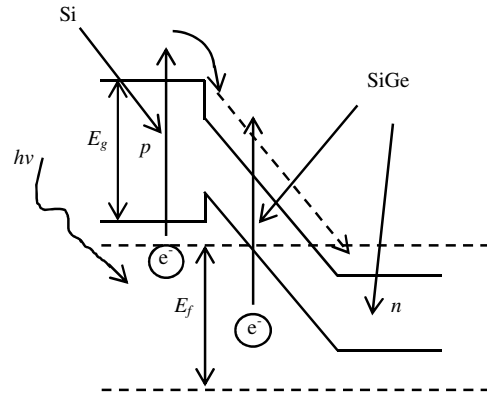**Fig. 5** Illustration of the diode-connected HBT used as a pixel.

Fig. 6 Band gap energy diagram of reverse-biased diode-connected silicon germanium (SiGe) HBT detector.

6 Experimental Verification

6.1 Prototype Design

The objective of this research was to improve DR and sensitivity in the near-IR band using BiCMOS technology instead of CCD technology most commonly used in gated IR detectors. A pixel is only one part of the detector, additional peripheral circuitry is required to be able to perform the gating readout function.

Figure 7 shows the block diagram of the implemented detector. AMS's high performance interface tool kits were used for the peripheral circuitry, since it is already optimized. Two different circuit topologies were implemented for noise measurements. The multiplexer (MUX) comprises of NAND3 gates, D flip-flops and inverters to operate the MOS transmission gate (TG) devices biased in the triode region. This operation processes the photon-generated currents to an acceptable output voltage.

The complete detector schematic for the multiple-pixel-single amplifier detector is given in Fig. 8.

In Fig. 8 it can be clearly seen that the complete array of pixels make use of only one output amplifier and a duty cycle. This reduces the component count at a cost of noise owing to the influence of the neighboring pixels on the current pixel being read whereas with only one pixel per output amplifier, the component count is increased but the switching noise is reduced. This reduction can be
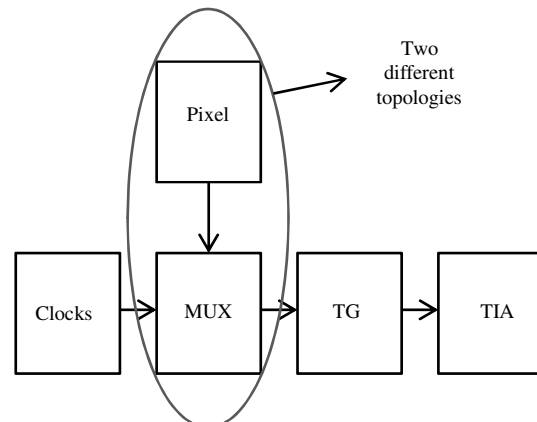

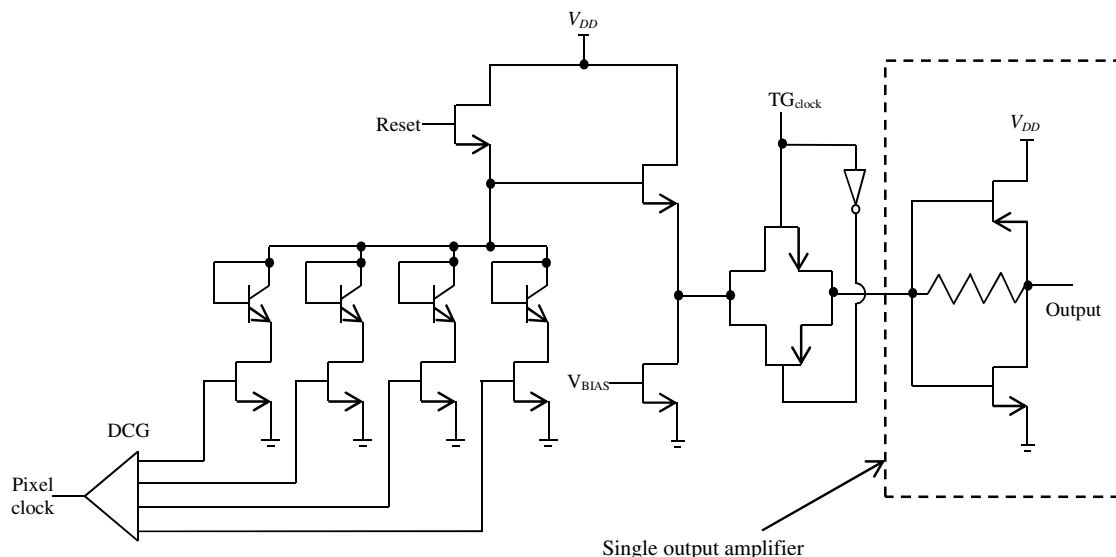**Fig. 7** Block diagram of the implemented detector.

Fig. 8 Complete detector schematic of the multiple-pixel single amplifier detector.

attributed to the lack of any influence from neighboring pixels. The experimental noise results presented in Sec. 7.1 verifies this.

The layout and chip photograph of the implemented detector are given in Fig. 9. Pixels were placed 1 mm from the edge so that they are in the center of the die to capture most light. The shape and placement of the detector was decided in order to accommodate two other projects (MPW).

6.2 Signal Analyzer

To be able to perform the noise measurements of the detector, a signal analyzer was used. The detector was connected as shown in Fig. 1.

Figure 1 shows the experimental setup used to obtain the necessary noise measurements. The results were de-embedded to obtain the noise of the detector. The signal analyzer used for this research is the SR785 from Stanford Research Systems. This system can measure noise up to 102 kHz noise frequency with an accuracy of 25 ppm
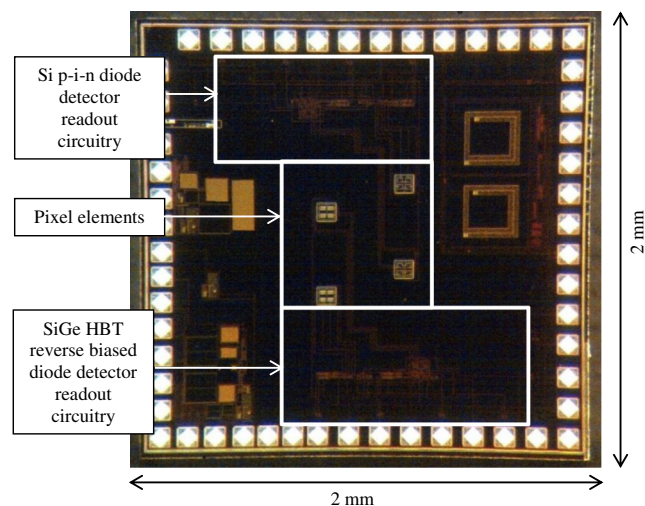

Fig. 9 Layout and chip photograph of the implemented detector.

from 20°C to 40°C. The system also exhibits a line resolution of 800 with an amplitude accuracy of 0.2 dB.

The LNA used was the SR560 also from Stanford Research Systems. This LNA exhibits an input noise of $4 \text{ nV}/\sqrt{\text{Hz}}$ with a 1 MHz bandwidth. The gain of the system can be varied from 1 to 50,000 V/V and it also comes equipped with a battery pack to eliminate noise peaks from a wall socket AC supply for example.

6.3 Monochromator

A monochromator was used to obtain the sensitivity measurements of the detector.

Figure 2 shows the experimental setup with the different subsystems required to perform the sensitivity measurements that make up the monochromator. A chopping frequency of 17 Hz was chosen for two reasons. The first is that it is not a harmonic of the supply frequency of 60 Hz (American power supplies) and the second is that the HBTs exhibit a very fast response time when radiated. This setup is also commonly used in the literature.

The monochromator used was the DK 480½ m monochromator from Digikröm. This monochromator exhibits a focal length of 480 mm with a wavelength precision and accuracy of 0.007 and 0.3 nm, respectively. It exhibits a 1200 g/mm grating with a maximum resolution of 0.03 nm and a scan speed of 1 to 1200 nm/min.

6.4 Dynamic Range Measurements

To measure the DR of the detector, two different quantities were required: the maximum voltage swing and the output noise. This required two different measurements and thus, with the available equipment, cannot be measured directly. The sensitivity and noise measurements were used to calculate the DR of the system using Eq. (1).

The reset noise was not measured because of the limited number of oscillators available and therefore the term $[2(kT/\alpha q)G_{C_{PH}}]$[13] was omitted because of the reset gain, which is 0, because no reset was done during the

measurement phase. The denominator represents the total output readout noise of the system.

6.5 Quantum Efficiency

Sensitivity measurements can be used to calculate the QE of the detector. The measured sensitivity is in V/W and first has to be converted to A/W. The resulting QE can be calculated using Eq. (5):[8]

$$QE(\eta) = \frac{1240R(\text{A/W})}{\lambda},\qquad(5)$$

where R is the measured sensitivity (A/W) and λ is the radiating wavelength (nm).

7 Measured Results

This section provides the details of the measurement results validating the reported work.

7.1 Noise Results

Figure 10 shows the noise results of both topologies of detectors. The results obtained are a function of noise frequency. The first few measurements up to 1 kHz are inconclusive owing to the signal analyzer stabilization and are thus omitted. The single-pixel single-amplifier detector exhibits lower noise compared to the multiple-pixel single-amplifier detector. This can be attributed to the influence of the neighboring nonfunctioning pixels on the pixel being read and processed. This was required to calculate the DR of the detector, as mentioned in Sec. 6.4.

7.2 Sensitivity Results

Figure 11 depicts the sensitivity results obtained practically and shows a peak sensitivity of 180 mA/W at a radiating wavelength of 665 nm for the SiGe HBT detector. At the same wavelength Si p-i-n diodes exhibit a sensitivity of 60 mA/W. This illustrates that Ge doping in a Si substrate indeed increases detection in the near-IR band. The second rise in sensitivity is due to harmonics. This must not be mistaken for a second detecting band. This was experimentally
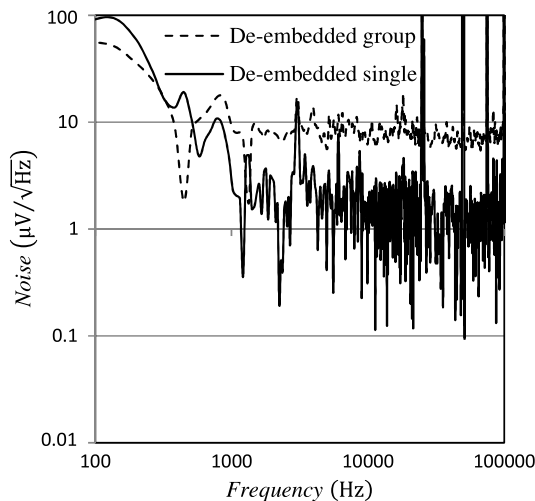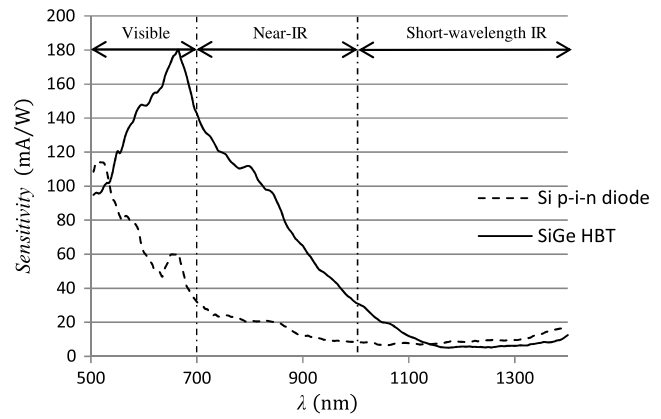

Fig. 11 Measured sensitivity results for both IR detectors.

verified by placing a radiation filter, which filters out any radiation with a wavelength of less than 1.6 μm.

7.3 Dynamic Range

The DR results were experimentally obtained by using the noise and sensitivity results. The DR was then calculated by using Eq. (1). The results are given below:

- $V_{\text{MAX}} - V_{\text{DARK}} = 117$ nV.
- Noise values in Fig. 10 were used. The reset pin was tied to V_{CC} and therefore no reset noise was present during the measurements owing to the availability of oscillators.

A value of 70 dB was recorded for the DR, which is an improvement based on what has been published in Table 2.

7.4 Quantum Efficiency

Figure 12 represents the calculated QE from the measured sensitivity by using Eq. (5) and shows that the maximum QE of the SiGe HBT detector is around 33%, which is slightly higher than published detectors in the literature in this band.

8 Experimentally Obtained Specifications

The complete characteristics of the implemented detector are summarized in Table 5.
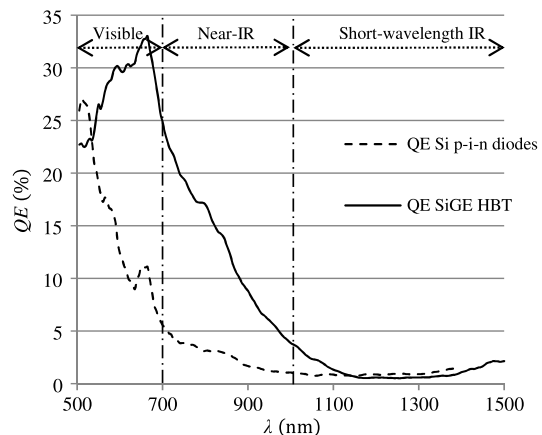

Fig. 10 De-embedded noise of both IR detectors.

Fig. 12 QE versus wavelength of prototyped detectors.

Table 5 Final prototype detector characteristics.

Characteristic	This work
Technology node	0.35 μm BiCMOS
Array size	2 × 2
Pixel size	6.6 × 11 μm^2
Noise	2 μV/$\sqrt{Hz}$
DR	70 dB
Sensitivity	180,000 V/W or 180 mA/W
Power consumption	10 mW

The pixel size was chosen large enough to capture a usable amount of IR radiation. The size of the pixel is directly proportional to the amount of output current produced but has no influence on the sensitivity or DR of the detector as it revolves around the output signal per watt of incident light which is size-independent. The power consumption is also very small, but that will increase when a larger array is prototyped. However, this will again have no influence on the sensitivity and DR.

9 Summary

An improvement in DR and responsivity in near-IR detectors is shown by using 0.35 μm SiGe HBT BiCMOS technology instead of CCD technology. An array of 2 × 2 pixels of size 6.6 × 11 μm^2 was fabricated. The output noise, DR, and sensitivity are not affected by the number of pixels, but rather the size of the pixels. A noise value comparable to Table 1 of 2 μV/$\sqrt{Hz}$ was recorded.

A DR value of 70 dB and peak responsivity value of 180 mA/W at a radiating wavelength of 665 nm (peak) were recorded for the SiGe HBT near-IR detector, which is a significant improvement compared to published detectors (both CCD and CMOS). This work also showed a shift in detecting band towards the near-IR band with IC technology. A further shift into the near-IR band is desired and could be achieved by either increasing the doping concentration of Ge in the Si wafer within allowable limits, or by using unconventional structures at integrated circuit level to capture near-IR radiation more effectively.

Acknowledgments

References

1. G. E. Smith, "The invention and early history of the CCD," *Nucl. Instrum. Methods Phys. Res. Sect. A* **607**(1), 1–6 (2009).
2. B. Rodricks et al., "A CMOS-based large-area high-resolution imaging system for high-energy X-ray applications," *Proc. SPIE* **7079**, 707914 (2008).
3. H. Fan et al., "Research of noise reduction and non-uniformity correction for CMOS image sensor," *Proc. SPIE* **7384**, 738423 (2009).
4. S. Kawahito, "Circuit and device technologies for CMOS functional image sensors," in *Proc. IFIP Int. Conf. on Very Large Scale Integration*, pp. 42–47, IEEE, Nice (2006).
5. N. Bassler, "Radiation damage in charge-coupled devices," *Radiat. Environ. Biophys.* **49**(3), 373–378 (2010).
6. G. C. Holst and R. G. Driggers, "Small detectors in infrared system design," *Opt. Eng. J.* **51**(9), 096401 (2012).
7. S. Yang et al., "An ultra low power CMOS motion detector," *IEEE Trans. Consum. Electron.* **55**(4), 2425–2430 (2009).
8. M. Bass, *Handbook of Optics, Fundamentals, Techniques, and Design*, 2nd ed., Vol. 1, McGraw-Hill Access Engineering, New York (2004).
9. E.L. Jacobs et al., "Concealed weapon identification using terahertz imaging," *Proc. SPIE* **6212**, 62120J (2006).
10. A. Theuwissen, "CMOS image sensors: state-of-the-art and future perspectives," in *Proc. of 33rd European Solid-State Device Research Conf.*, pp. 21–27, IEEE, Munich (2007).
11. S. Eminoglu, M.Y. Tanrikulu, and T. Akin, "A low-cost 128 × 128 uncooled infrared detector array in CMOS process," *J. Microelectromech. Syst.* **17**(1), 20–30 (2008).
12. R. Yun and M. Joyner, "A monolithically integrated phase-sensitive optical sensor for frequency-domain NIR spectroscopy," *IEEE Sens. J.* **10**(7), 1234–1242 (2010).
13. F. Schuster et al., "Broadband terahertz imaging with highly sensitive silicon CMOS detectors," *Opt. Express* **19**(8), 7827–7832 (2011).
14. P. Martin-Gonthier et al., "Dynamic range optimisation of CMOS image sensors dedicated to space applications," *Proc. SPIE* **6744**, 67440U (2007).
15. A. El Gamal and H. Eltoukhy, "CMOS image sensors," *IEEE Circ. Dev. Mag.* **21**(3), 6–20 (2005).
16. R. Berger et al., "A 64 × 64-pixel CMOS test chip for the development of large-format ultra-high-speed snapshot imagers," *IEEE J. Solid State Circ.* **43**(9), 1940–1950 (2008).
17. C. Li, F. Gong, and P. Wang, "A low-power ultrawideband CMOS power detector with an embedded amplifier," *IEEE Trans. Instrum. Meas.* **59**(12), 3270–3278 (2010).
18. O. Fidaner et al., "Ge–SiGe quantum-well waveguide photodetectors on silicon for the near-infrared," *IEEE Photon. Technol. Lett.* **19**(20), 1631–1633 (2007).
19. Virginia Semiconductor Inc., "Optical properties of SiGe and Ge," http://www.virginiasemi.com/pdf/Optical%20Properties%20fo%20SiGe%20and%20Ge.pdf.

Johan Venter is a graduate student member, *IEEE*, and serves CEFIM, Department: Electrical, Electronic and Computer Engineering, University of Pretoria, Pretoria, South Africa on a part-time basis. He serves as an assistant lecturer, but engages in a doctorate-level study on a full-time basis. His postgraduate research interest includes taking forward new Si- and SiGe-based transistor level base technology for photodetectors.

Saurabh Sinha, *SMIEEE*, is an electrical engineer, a researcher, and an educator. In 2007, he received the South African Institute of Electrical Engineers Engineer of the Year Award. More recently, he received the 2010 University of Pretoria Laureate Award, the most esteemed alumni award. For more than a decade, he has been with the University of Pretoria, where he serves as the director of CEFIM. Together with his group, he conducts teaching at undergraduate and postgraduate levels, research, and associated management tasks. He has authored or coauthored over 60 publications in peer-reviewed journals and at international conferences. He is the managing editor of the *SAIEE Africa Research Journal*. Beyond his academic contributions, he serves as an industrial consultant for Business Enterprises at University of Pretoria (Pty) Ltd.